FULL PAPER

Quantification of Quantum Efficiency and Energy Losses in Low Bandgap Polymer:Fullerene Solar Cells with High Open-Circuit Voltage

Koen Vandewal, Zaifei Ma, Jonas Bergqvist, Zheng Tang, Ergang Wang, Patrik Henriksson, Kristofer Tvingstedt, Mats R. Andersson, Fengling Zhang, and Olle Inganäs**

In organic solar cells based on polymer:fullerene blends, energy is lost due to electron transfer from polymer to fullerene. Minimizing the difference between the energy of the polymer exciton (E_{D^*}) and the energy of the charge transfer state (E_{CT}) will optimize the open-circuit voltage (V_{oc}). In this work, this energy loss E_{D^*}-E_{CT} is measured directly via Fourier-transform photocurrent spectroscopy and electroluminescence measurements. Polymer:fullerene photovoltaic devices comprising two different isoindigo containing polymers: P3TI and PTI-1, are studied. Even though the chemical structures and the optical gaps of P3TI and PTI-1 are similar (1.4 eV–1.5 eV), the optimized photovoltaic devices show large differences in V_{oc} and internal quantum efficiency (IQE). For P3TI:$PC_{71}BM$ blends a E_{D^*}-E_{CT} of ~ 0.1 eV, a V_{oc} of 0.7 V and an IQE of 87% are found. For PTI-1:$PC_{61}BM$ blends an absence of sub-gap charge transfer absorption and emission bands is found, indicating almost no energy loss in the electron transfer step. Hence a higher V_{oc} of 0.92 V, but low IQE of 45% is obtained. Morphological studies and field dependent photoluminescence quenching indicate that the lower IQE for the PTI-1 system is not due to a too coarse morphology, but is related to interfacial energetics. Losses between E_{CT} and qV_{oc} due to radiative and non-radiative recombination are quantified for both material systems, indicating that for the PTI-1:$PC_{61}BM$ material system, V_{oc} can only be increased by decreasing the non-radiative recombination pathways. This work demonstrates the possibility of obtaining modestly high IQE values for material systems with a small energy offset (<0.1 eV) and a high V_{oc}.

1. Introduction

Extensive research in the last years has increased the power conversion efficiency (PCE) of organic solar cells up to 7–8%.[1,2] Organic solar cells utilizing a polymer as electron donor and a fullerene derivative as electron acceptor are among the most studied and highest efficiency systems. Some polymer:fullerene blends or bulk heterojunctions yield absorbed-photon-to-collected-electron quantum efficiencies or internal quantum efficiencies (IQE) close to 100% at short circuit.[3,4] A crucial step in obtaining a high yield of free charge carriers upon illumination in these systems, is electron transfer at the organic/organic heterointerface.[5,6] Minimizing the energy lost in this indispensable electron transfer step is important for increasing the PCE of this type of potentially cheap and flexible solar cells further and beyond 10%.[7–9]

The lost energy as a consequence of charge transfer is reflected in a reduction of the open-circuit voltage (V_{oc}) of the solar cell: while the maximum obtainable short-circuit current (J_{sc}) is determined by the optical gap of the main absorber, the maximum obtainable V_{oc} can be related to the energy of the interfacial electronic state in which the charge is transferred.[9–14] In the case that the donor material is the main absorber, the energy lost due to the electron transfer is given by the difference between the energy of the excited donor (E_{D^*}) and the energy of the charge transfer (CT) state (E_{CT}).

Experimentally, E_{CT} has been determined by optical methods probing weakly allowed CT state absorption[10–13] and emission[14–16] or has been estimated as the difference between the highest occupied molecular orbital (HOMO) of the donor and lowest unoccupied molecular orbital (LUMO) of the acceptor.[7,8,17] The energy lost in the electron transfer step (E_{D^*}-E_{CT}) similarly is often approximated by difference in LUMOs of the donor and acceptor material.[7,8] However estimations of the relevant energetics based on frontier orbital energies inferred from measurements on the isolated donor and acceptor, neglect the influence of exciton binding energy and other interfacial effects.[18] In this work we therefore determine

Dr. K. Vandewal,[†] Z. Ma, J. Bergqvist, Z. Tang, Dr. K. Tvingstedt, Dr. F. Zhang, Prof. O. Inganäs
Biomolecular and Organic Electronics
Department of Physics
Chemistry and Biology
Linköping University
Linköping, 58183, Sweden
E-mail: vandewal@stanford.edu; ois@ifm.liu.se
Dr. E. Wang, P. Henriksson, Prof. M. R. Andersson
Department of Chemical and Biological Engineering/Polymer Technology
Chalmers University of Technology
Göteborg, 41296, Sweden
[†] Present address: Department of Materials Science and Engineering, Geballe Laboratory for Advanced Materials, 239 McCullough Building, Stanford University, Stanford, CA 94305, USA

DOI: 10.1002/adfm.201200608

PTI-1 P3TI

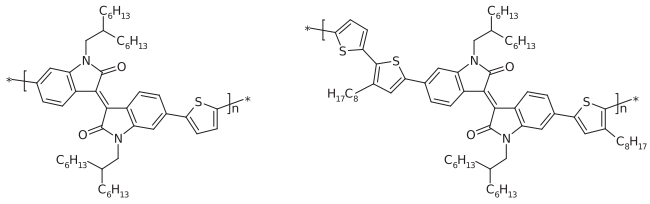

Scheme 1. The chemical structures of PTI-1 and P3TI.

interfacial pair energies and offset energies directly on photovoltaic devices through the use of sensitive optical methods.

Detailed studies on the influence of the D-A energy offsets have shown that a smaller energy lost in the electron transfer step correlates with a lower yield of free charge carriers generated per absorbed photon.[19,20] These observations have lead to discussions on the role of vibrational excess energy on the free charge carrier generation process[21–23] and the influence of intersystem crossing to triplet excitons on donor or acceptor.[24–26]

Because of the major importance of minimizing the energy lost in the electron transfer step, we perform in this paper a detailed investigation of two polymer:fullerene systems with a low E_{D^*}-E_{CT} difference. The donor polymers P3TI and PTI-1 explored in this work are based on the isoindigo functional group and have similar chemical structures (**Scheme 1**) and optical gaps E_{D^*} (1.4–1.5 eV). However, when blended with the fullerene derivatives $PC_{61}BM$ and $PC_{71}BM$, we find substantial differences in E_{CT}, V_{oc} and IQE. P3TI:$PC_{71}BM$ devices have an IQE of ~87% and a V_{oc} of 0.7 V, with an optimized device PCE of 6.3%.[27] For the second polymer, PTI-1, we found $PC_{61}BM$ to be the optimal acceptor, achieving a PCE of 4.5%.[28] Although the PTI-1:$PC_{61}BM$ system has a higher V_{oc} (0.92 V) than the P3TI:$PC_{71}BM$ system, the IQE (~45%) is lower.

We investigate the morphology of both polymer:fullerene blends with Atomic Force Microscopy (AFM) and Transmission Electron Microscopy (TEM) and find that the addition of 1,8-diiodooctane (DIO) as a processing additive removes fullerene rich regions and makes the blends more homogenous on the tens of nanometers scale. The resulting morphologies of the optimized PTI-1 and P3TI based blends appear very similar, within the resolution of these techniques.

Voltage dependent photoluminescence studies reveal that in the power generating quadrant and under illumination, the P3TI:$PC_{71}BM$ interface quenches polymer excitons more efficiently than the PTI-1:$PC_{61}BM$ interface. However, when applying sufficiently high negative voltages, quenching of PTI-1 photoluminescence (PL) in PTI-1:$PC_{61}BM$ blends becomes more efficient, while quenching of P3TI excitons in P3TI:$PC_{71}BM$ blends remains unaffected by the electric field. This indicates that the lower IQE obtained for PTI-1:$PC_{61}BM$ blends is due to the hampered ability of the PTI-1:$PC_{61}BM$ interface to generate charge carriers at the low electric fields present in the power generating quadrant.

We use Fourier-transform photocurrent spectroscopy (FTPS) and electroluminescence (EL) spectra in order to quantify the energies E_{D^*} and E_{CT}. We find for the P3TI:$PC_{71}BM$ an E_{D^*}-E_{CT} difference of ~0.1 eV. For the PTI-1:$PC_{61}BM$ system, pure polymer and CT absorption and emission bands cannot be distinguished indicating an even lower E_{D^*}-E_{CT}, close to 0.0 eV. We speculate that this lack of driving force for electron transfer in the PTI-1:$PC_{61}BM$ system is the origin of the decreased IQE as compared to the P3TI:$PC_{71}BM$ system.

The V_{oc} under solar illumination for both material systems is about 0.6–0.7 V lower than E_{CT}/q. By using the relations between CT absorption, quantum efficiency of EL emission and V_{oc}, we find that for both material systems ~0.2 eV of this loss can be attributed to radiative recombination through the CT state and 0.4–0.5 eV is due to additional non-radiative recombination pathways. The magnitude of these losses are typical for polymer:fullerene systems.[9–13]

This investigation implies that, apart from the unknown non-radiative recombination loss, the V_{oc} of PTI-1:$PC_{61}BM$ is optimized. Even though there is virtually no driving force for electron transfer, still a modestly high IQE of ~45% can be achieved in this material system.

2. Electro-Optical Characterization of P3TI and PTI-1 and Their Blends with $PC_{71}BM$ and $PC_{61}BM$

2.1. Absorption Coefficients

For this work we use PTI-1 and P3TI batches with number average molecular weights (M_n) of respectively 48 000 and 73 000, and polydispersity index of 2.7 and 3.0. **Figure 1** shows the absorption coefficient determined by variable angle spectroscopic ellipsometry (VASE), for films spincoated from *ortho*-dichlorobenzene (*o*-DCB) of PTI-1, P3TI and their blends with respectively $PC_{61}BM$ and $PC_{71}BM$ in a 2:3 weight ratio.

For both pure materials the absorption coefficient is highest in the low energy region between 580 and 720 nm. PTI-1 peaks at 633 nm and 680 nm, while P3TI peaks at 647 nm. For polymers with donor and acceptor segments on the repeating unit, the lowest energy bands are often attributed to an intramolecular, charge transfer like transition.[29,30] Maximum absorption coefficients for PTI-1 and P3TI are 1.4×10^5 cm^{-1} and 1.2×10^5 cm^{-1} respectively, which are rather high for such low optical gap materials. This makes these materials particularly interesting for photovoltaic applications. In the 350–500 nm region, local maxima with lower absorption coefficients can be found for both pure materials. Blending these polymers with the fullerene derivatives $PC_{61}BM$ and especially $PC_{71}BM$ increases the relative absorption in the high-energy region.

P3TI yields the best device performance when combined with $PC_{71}BM$ in a 2:3 weight ratio. PTI-1 gives better performance with $PC_{61}BM$, despite its lower absorption coefficient than $PC_{71}BM$. We previously attributed this to a better miscibility of PTI-1 with $PC_{61}BM$ than $PC_{71}BM$.[28] Therefore, in the remainder of the text we compare P3TI:$PC_{71}BM$ devices with PTI-1:$PC_{61}BM$ devices both in a 2:3 weight ratio.

For both pure and blend devices, also the refractive index as a function of wavelength was determined by VASE and shown in supplementary Figure S1. For all materials the refractive index is around 1.9 in the energy range below the optical gap of the

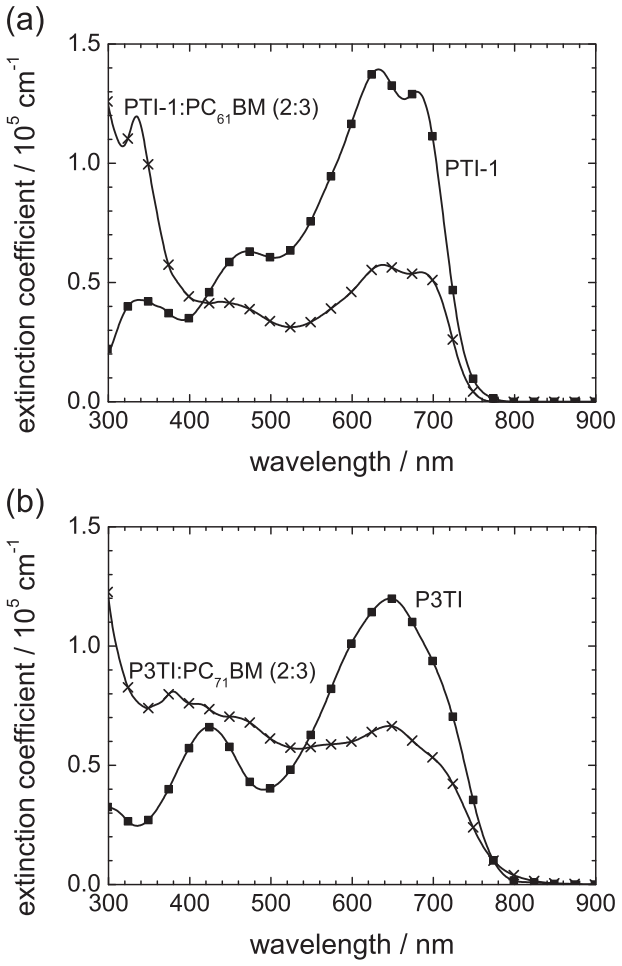

Figure 1. The absorption coefficient of (a) PTI-1 (squares), PTI-1:$PC_{61}BM$ (2:3) (crosses) and (b) P3TI (squares), P3TI:$PC_{71}BM$ (2:3) (crosses) determined by VASE.

polymers. This data is used below for the determination of the IQEs of the devices discussed below.

2.2. Photovoltaic Devices

Photovoltaic devices in the standard configuration with the active layer sandwiched between ITO/PEDOT:PSS and LiF/Al electrodes were prepared. As active layers we investigate not only the PTI-1:$PC_{61}BM$ and P3TI:$PC_{71}BM$ blends but also the pure polymers. Device comprising blends have an active layer thickness of ~90 nm, those comprising pure polymers are slightly thinner (~80 nm). In order to optimize the morphology of the blends, the processing additive DIO (2.5% by volume) was added to the *o*-DCB solutions.

Devices comprising PTI-1:$PC_{61}BM$ (2:3) as active layer are modestly good solar cells with a high V_{oc} of 0.92 V and FF of 0.63 under solar illumination. For the batch of devices studied in this work we obtain a J_{sc} of typically around only 5.7 mA.cm^{-2}. Using $PC_{71}BM$ as acceptor yields similar V_{oc} and FF but decreases J_{sc} even further.[31]

Devices with P3TI:$PC_{71}BM$ (2:3) as active layer have a lower V_{oc} (0.7 V) than the PTI-1:$PC_{61}BM$ devices. The FF is similar for both polymers but J_{sc} is more than doubled, yielding 12.9 mA.cm^{-2} for the P3TI:$PC_{71}BM$ devices investigated in this study. Again, V_{oc} and FF for P3TI based devices are independent of the use of $PC_{61}BM$ or $PC_{71}BM$.

When the pure materials are used as active layer, J_{sc} is about 5×10^2 times lower than the J_{sc} of the blends. The V_{oc} for the pure materials however are 0.96 V and 0.88 V for respectively PTI-1 and P3TI, which are higher as compared to the V_{oc} for the blends. A detailed analysis of the V_{oc} for both pure and blend devices and its relation to optical gaps is given and discussed further down this paper.

External quantum efficiency (EQE) and IQE of pure and blend devices are shown in **Figure 2**. IQE as a function of wavelength λ was, as outlined in ref. 32, calculated using the measured EQE, the measured device reflectance $R_{cell}(\lambda)$ and the parasitic electrode absorptance $A_{par}(\lambda)$ obtained from optical transfer matrix modeling according to:

$$IQE(\lambda) = \frac{EQE(\lambda)}{1 - R_{cell}(\lambda) - A_{par}(\lambda)} \quad (1)$$

Wherein the absorption coefficients and refractive indexes used in the optical model were determined by VASE.

For the devices comprising the pure polymers as active layers, the overall EQE is low (Figure 2b), with substantial variations from device to device. Focusing on the spectral shape of the EQE, it is observed that, surprisingly, in the wavelength region where the polymers have their lowest energy absorption band (580 nm–720 nm) EQE is lowest. In the higher energy region below 580 nm EQE rises for decreasing wavelengths. This is due to the fact that the IQE of the devices made of pure polymers only is not at all constant (Figure 2d), but has a very strong dependence on wavelength: the IQE in the low energy absorption band is approximately 100 times lower than IQE in the short wavelength region. This observation is valid for devices comprising both pure PTI-1 and P3TI as active layers. Such non-constant IQE over the wavelength range of absorption has been observed before for pure polymers comprising donor and acceptor moieties on the repeating unit.[33] In those cases however, the effect was not as strong as observed here. Additionally, the spectral response of devices comprising polymer only, can be influenced by the application of a reverse bias: The photocurrent rises faster with the application of a negative voltage (increasing electric field) in the low energy spectral region than in the high-energy spectral region. (**Figure 3**a,b)

This observation indicates that photocurrent generation in the pure isoindigo based polymers is strongly dependent on the nature of the primary excited state: For excitation in the high energy absorption bands photocurrent generation is more efficient and less reverse bias dependent than for excitation in the low energy absorption bands. However, even for the high-energy excitations, the overall IQE for these polymer only devices remains low (<1.5%)

When blending the polymers with fullerenes however the situation gets completely different: IQE now becomes constant over all absorbing wavelengths (Figure 2 (c)), and no substantial reverse bias voltage spectral dependence can be observed

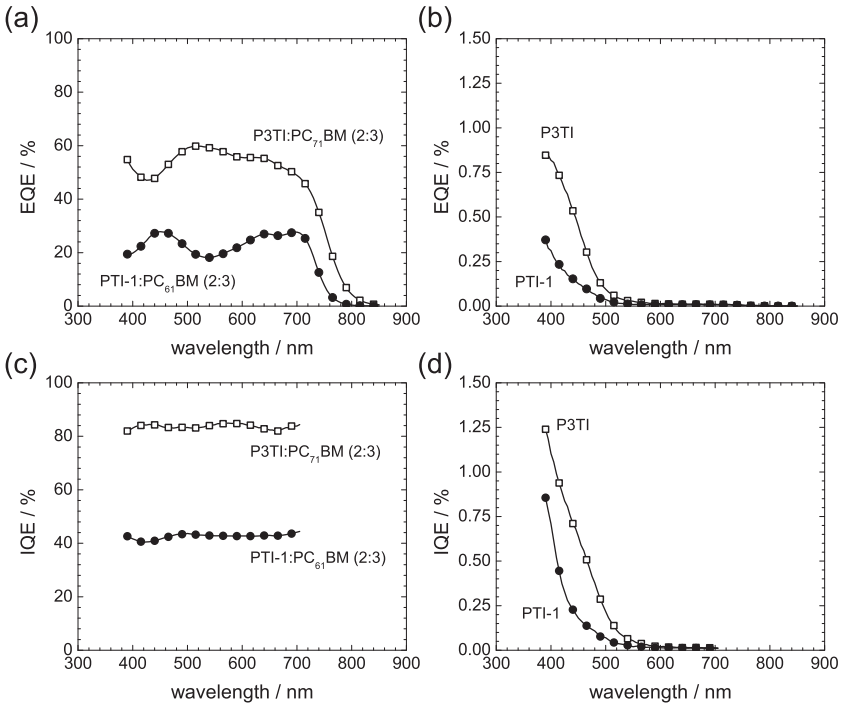

Figure 2. The EQE spectra for typical photovoltaic devices comprising (a) PTI-1:$PC_{61}BM$ (2:3) (closed symbols) and P3TI:$PC_{71}BM$ (2:3) (open symbols) (b) pure PTI-1 (closed symbols) and pure P3TI (open symbols). The IQE for both blend and pure polymer devices are shown in panel (c) and (d).

anymore (Figure 3c and d). This indicates that a new dominating dissociation pathway independent of excitation energy is present in the polymer:fullerene blends. The EQE goes up to a maximum of ~30% for the PTI-1:$PC_{61}BM$ device and ~60% for the P3TI:$PC_{71}BM$ device (Figure 2a). This results in an IQE of 45% for the PTI-1:$PC_{61}BM$ based device and 87% for the P3TI:$PC_{71}BM$ based device over the strongly absorbed wavelengths (Figure 2c).

Considering the similar chemical structures and optical properties of PTI-1 and P3TI, it is remarkable that IQE and V_{oc} for the optimized photovoltaic devices differ so much. A first explanation of non-optimal performance of polymer:fullerene blends is often sought in non-optimal morphology of the active layer. However, low performance of organic donor-acceptor (D-A) devices can in principle also be due to an increased geminate recombination, i.e. the recombination of CT states formed following immediately upon electron transfer. In what follows, we attempt to disentangle these reasons. We do so by probing morphological properties by TEM and AFM. D-A interfacial properties and CT state energetics are studied by PL measurements under different bias voltages and spectrally resolved EL and FTPS measurements.

3. Morphological Characterization with AFM and TEM

In order to study if the difference in photocurrent generation and IQE between the devices based on PTI-1 and P3TI has a morphological origin, AFM and TEM studies have been carried out. In order to obtain the best performing devices, the solution processing additive DIO, was used.[27,28,31] The effect of DIO on the nano-scale morphology of the active layers is also investigated.

Figure 4a and c show AFM images of the active layers processed from *o*-DCB without DIO. Obvious big domains, on the order of 100 nm in diameter, indicate that a possible large phase separation exits in both P3TI:$PC_{71}BM$ and PTI-1:$PC_{61}BM$ active layers, diminishing device performance.[27,28,31] However, the active layers casted from *o*-DCB with the addition of 2.5% (by volume) DIO (Figure 4b and d) show a much finer structure with a RMS value of 4.5 nm and 1.5 nm for PTI-1 and P3TI based active layer, respectively.

These results are confirmed by the TEM images shown in **Figure 5**: For the active layers processed without DIO (Figure 5a and c), clear phase separation can be observed. The addition of DIO (Figure 5b and d) leads to the formation of a much finer morphology. The big domains have disappeared for both the P3TI:$PC_{71}BM$ and PTI-1:$PC_{61}BM$ blends. Similar effects of solvent additives have been observed for different polymer:fullerene systems.[34–36]

Although the large scale phase separation is eliminated in both PTI-1and P3TI based active layers with the help of DIO, and device performance is improved for both active layers, there is still a large difference in the IQE of the photovoltaic devices. However, there seem to be minor morphological differences between the active layers based on P3TI:$PC_{71}BM$ and PTI-1:$PC_{61}BM$ processed with DIO. The PTI-1 based active layer could be regarded as bit more homogenous as compared to the P3TI based active layer. However, the IQE of the latter device is larger. In order to investigate the ability of excitons to reach a polymer:fullerene interface, we will investigate PL quenching of both blends, processed with and without DIO, in the next paragraph.

4. Photoluminescence Quenching

In **Figure 6**a and b, PL spectra of the pure polymers PTI-1 and P3TI are compared with spectra of their blends with $PC_{61}BM$, respectively $PC_{71}BM$, processed with and without DIO. Films were spin-coated on glass and the excitation wavelength was 633 nm. For each polymer, the relative number of counts for the pure material and blend are corrected for differences in absorption at 633 nm and can hence be directly compared to each other. One can immediately see that for all blend material systems, pure polymer PL quenching upon the addition of fullerene is by no means complete.

For PTI-1, without and with the use of DIO, a surprisingly high fraction of respectively ~50% and ~30% of the PTI-1 PL

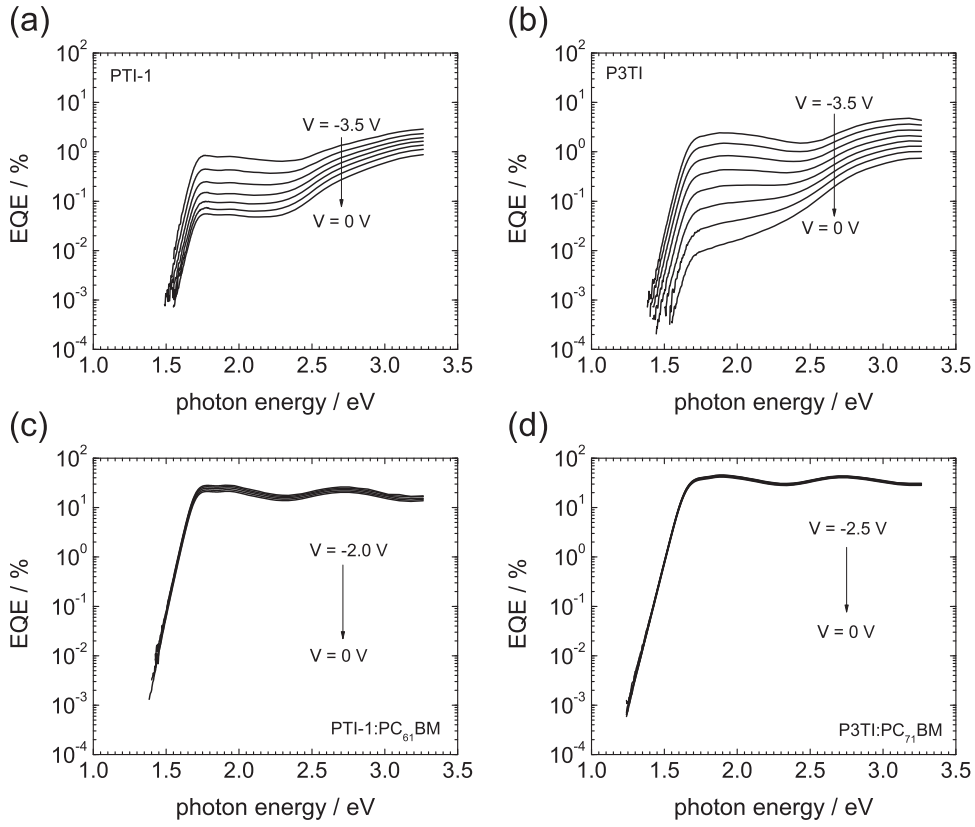

Figure 3. EQE spectra measured at different reverse bias voltages for (a) PTI-1, (b) P3TI, (c) PTI-1:$PC_{61}BM$ and (d) P3TI:$PC_{71}BM$. The spectral shape of the pure polymers depends strongly on bias voltage, while for the blends the spectral shape remains unchanged over the whole energy range of absorption, when changing the voltage.

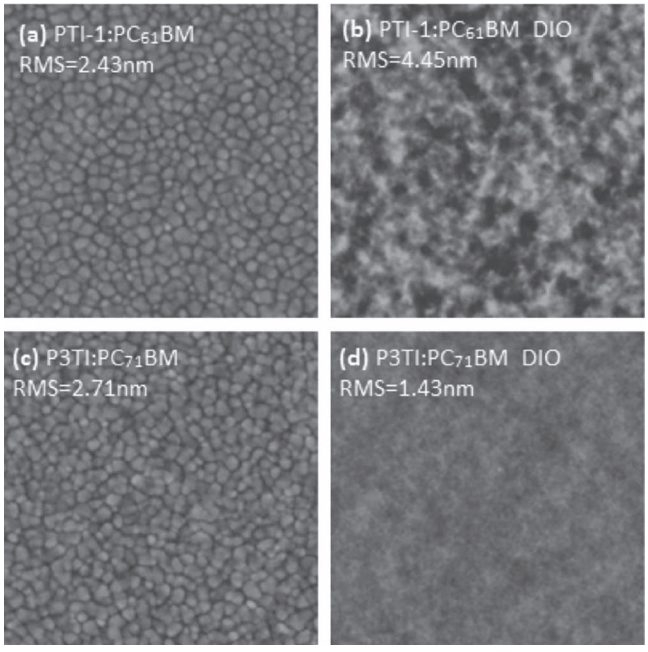

Figure 4. AFM images (5 × 5 μm) for (a) PTI-1:$PC_{61}BM$ prepared without DIO, (b) PTI-1:$PC_{61}BM$ prepared with DIO, (c) P3TI:$PC_{71}BM$ prepared without DIO and (d) P3TI:$PC_{71}BM$ prepared with DIO.

remains after blending with $PC_{61}BM$. In the P3TI:$PC_{71}BM$ blend, the PL is quenched stronger with ~15% (without DIO) and ~7% (with DIO) of the initial amount of P3TI PL counts remaining. Noteworthy is that PL of the pure polymers is already a very inefficient process: Using an integrating sphere we determine the PL quantum efficiency for both PTI-1 and P3TI to be 0.1%–0.5%.

The quenching of PL upon the addition of a fullerene acceptor is often considered to reflect the ability of polymer excitations to reach the polymer:fullerene interface within their lifetime. However, PL in polymer:fullerene blends can also originate from interfacial CT states. Direct radiative decay of CT states will result in a redshifted emission spectrum as compared to the pure polymer emission.[14,37–40] For systems with a low E_{D^*}-E_{CT}, such as those studied in this work, repopulation of the donor excited state with subsequent emission can occur and forms an indirect, radiative decay pathway for CT states.[16]

For the material systems studied in this work, no substantial spectral shifts in PL are observed for the blends as compared to the pure polymers, indicating most observed emission originates from polymer emission. In order to determine if this remaining emission is produced by repopulation of the polymer excited state via the indirect mechanism or originates from isolated, pure polymer domains, we perform a study of

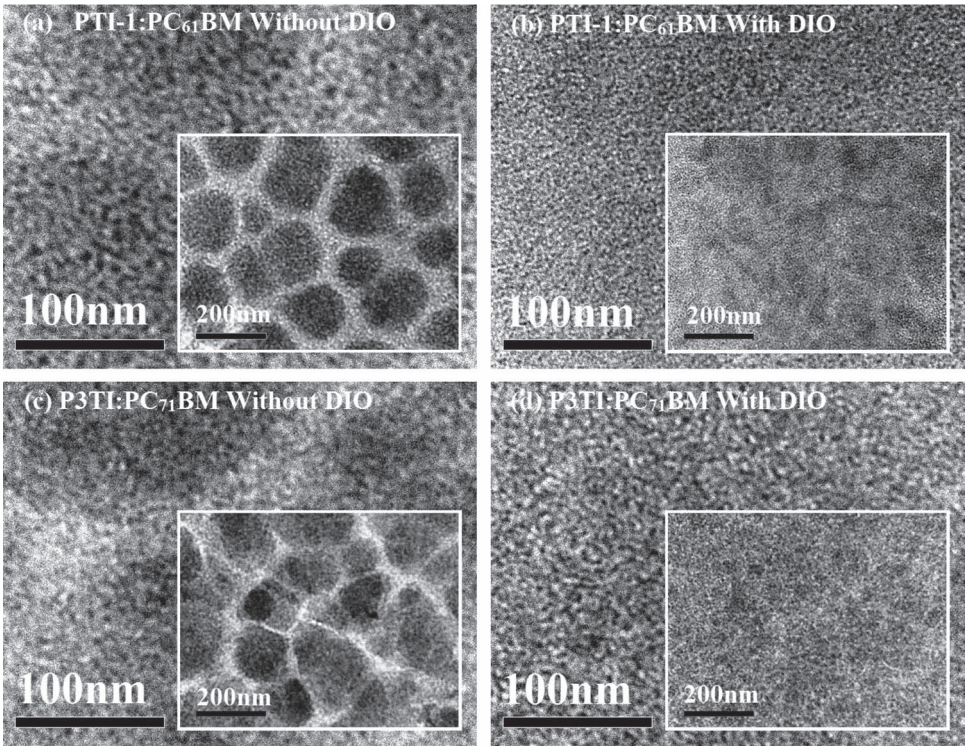

Figure 5. TEM images for (a) PTI-1:$PC_{61}BM$ (2:3) prepared without DIO, (b) PTI-1:$PC_{61}BM$ (2:3) prepared with DIO, (c) P3TI:$PC_{71}BM$ prepared without DIO and (d) P3TI:$PC_{71}BM$ prepared with DIO. The corresponding lower magnification TEM topographies are shown in the insets.

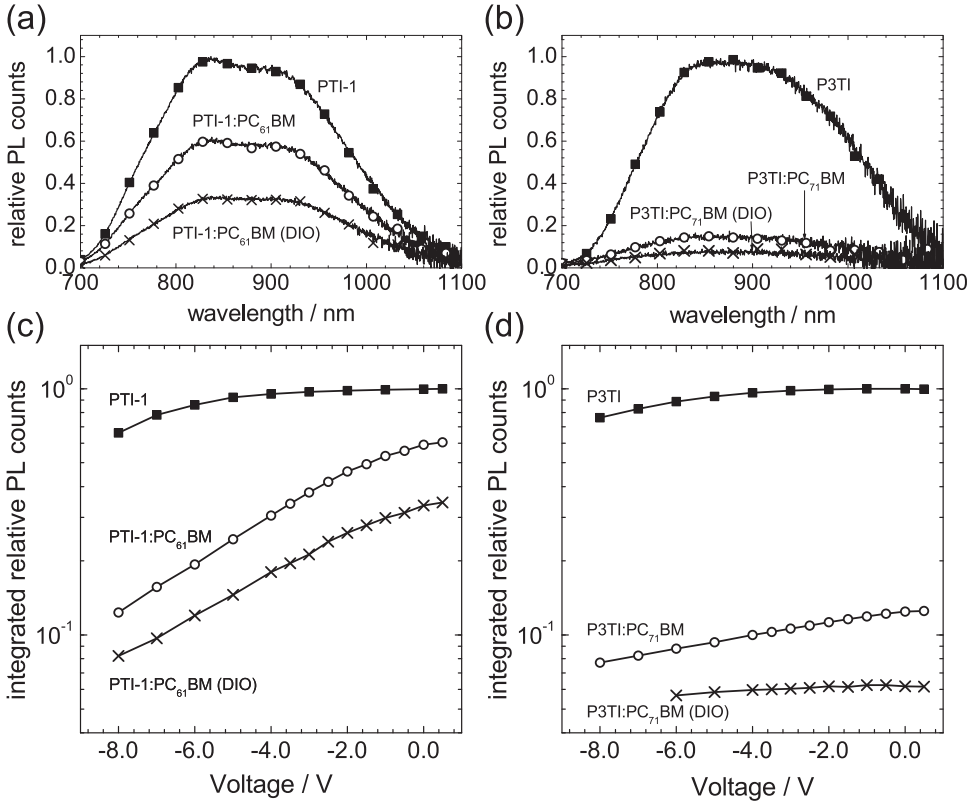

Figure 6. PL spectra of pure polymer films (squares) and blend films prepared without DIO (open circles) and with DIO (crosses). Spectra of (a) PTI-1 blends and (b) P3TI blends are shown relative to the pure material emission spectra. The integrated, relative PL counts for devices under a reverse bias voltage are shown in panel (c) for PTI-1 and (d) P3TI and their blends prepared with and without DIO.

the PL while varying the electric field (negative bias voltage) over the device.

Figure 6c and d show the integrated number of PL of counts as a function of applied voltage over photovoltaic devices comprising pure and blend active layers, processed with and without DIO. For devices comprising pure polymers, no substantial PL quenching is observed for voltages higher than –6 V.[40]

For the PTI-1:$PC_{61}BM$ (2:3) devices, processed with and without DIO, however, a different behavior can be observed. The substantial amount of PL counts remaining upon blending, can be reduced by applying negative voltages: The application of –6 V quenches the PL to a value of less than 35% of the PL counts around 0 V.

Contrary to this, for the P3TI:$PC_{71}BM$ device processed with DIO, a voltage dependence of the PL is basically absent: At –6 V still 95% of the emission present at 0 V remains. However for this blend, the polymer emission was already strongly quenched by the addition of fullerene. The P3TI:$PC_{71}BM$ devices processed without DIO, form an intermediate case for which a small dependence of the PL on bias voltage can be observed. For all material systems, we observe no changes in the spectral shape upon the application of the negative bias (supplementary Figure S2.).

The fact that we can quench the PTI-1:$PC_{61}BM$ emission with lower electric fields than needed for quenching the pure PTI-1 emission implies that a large part of the PL in the blend devices originates from donor excitations, repopulated from CT states which dissociate more efficiently when sufficiently high negative voltages are applied. For the P3TI:$PC_{71}BM$ blends, CT state dissociation is already relatively efficient at low voltages in the fourth quadrant, indicated by an overall higher quenching efficiency and IQE than in the PTI-1:$PC_{61}BM$ case. Application of negative voltages therefore results in only a small increase in quenching efficiency for P3TI:$PC_{71}BM$ blends processed without DIO and no increase in quenching efficiency for P3TI:$PC_{71}BM$ blends processed with DIO.

The analysis in this paragraph and the previous one, indicates that the poorer quenching of the PL and lower IQE for the PTI-1:$PC_{61}BM$ devices as compared to the P3TI:$PC_{71}BM$ devices originates mainly from a lower efficiency of interfacial CT state dissociation and not from a coarser morphology.

5. Determination of the Relevant Energy Levels and Relation to Photovoltaic Parameters

5.1. Determination of E_{D^*}-E_{CT} and Effect on IQE

The difference in V_{oc} of PTI-1:$PC_{61}BM$ and P3TI:$PC_{71}BM$ indicates that the energy of the CT state is different for these two material systems.[10,41] Weak light absorption by CT states can be detected by a highly sensitive measurement of the EQE spectrum in the sub-gap region.[10–12] Forward biasing a photovoltaic device can further be used to detect light emission by CT states: The injected charges will recombine at the polymer-fullerene interface forming a CT state, which can decay subsequently with the emission of a photon.[13–16] The weak oscillator strength and the low quantum efficiency ($<10^{-6}$) of radiative recombination via the CT state make both CT absorption and emission a weak process, but detectable with sensitive enough techniques.

Figure 7a and b show the low energy range of normalized EQE spectra as measured by the sensitive technique FTPS (FTPS-EQE) of pure and blend photovoltaic devices. Pure PTI-1 and P3TI have a pretty broad absorption onset in the range 1.4 eV–1.5 eV. Blending P3TI with $PC_{71}BM$ results in a slight redshift and further broadening of the absorption tail, making it possible to measure an EQE signal all the way down to 1.1 eV. Corresponding to previous observations of sub-polymer gap CT absorption in polymer:fullerene blends, we relate this additional absorption to the P3TI:$PC_{71}BM$ interface, as previously[10–12] and assign it to CT absorption. The addition of DIO to the processing solution results in a slight redshift of the CT band. For devices consisting of PTI-1 and PTI-1:$PC_{61}BM$ the absorption tail of pure PTI-1 and PTI-1:$PC_{61}BM$ look very similar and no extra, sub gap CT absorption band can be distinguished for the blends, processed with or without DIO. The presence of sub-gap CT absorption bands is very common for polymer:fullerene blends yielding a decent photocurrent generation.[10–12,42–45] Absence of a sub-gap CT state with energy lower than the singlets of the blend constituents has been previously associated with poor CT state population, and hence poor photocurrent generation.[9,45,46] Therefore, the absence of sub-gap CT absorption in the PTI-1:$PC_{61}BM$ system, which is a rather decently performing photovoltaic material, must thus be considered as exceptional.

Figure 8c and d show the electroluminescence spectra of pure and blend devices. For P3TI, the P3TI:$PC_{71}BM$ blends EL spectrum is redshifted as compared to the pure spectrum, by about 0.05 eV when no DIO was added to the processing solution and 0.1 eV in the case DIO was added. The quantum efficiency of EL is very low, both for pure P3TI and the blends, 1×10^{-7} and 5×10^{-9} respectively. For the PTI-1 material system, processed with and without DIO, the blends EL spectrum does not differ much from the pure materials spectrum. EL quantum efficiencies for both pure material and blends again are very low, respectively 1×10^{-6} and 1×10^{-7}.

From the EL and FTPS-EQE spectra, we estimate the offset E_{D^*}-E_{CT} ~0.1 eV for the optimized P3TI:$PC_{71}BM$ system, processed with DIO, while for PTI-1:$PC_{61}BM$ E_{D^*}-E_{CT} is smaller or equal to 0.0 eV. The fact that E_{CT} is so close to E_{D^*} for the PTI-1:$PC_{61}BM$ system, implies that population of the CT state becomes energetically less favorable. If CT states are populated, back electron transfer to the polymer singlet excited state becomes plausible, and can be in direct competition with CT state dissociation into free charge carriers.[16] Applying an electric field, as in the field quenching studies of the previous paragraph, will affect the CT state dissociation rate, reducing polymer exciton repopulation and quenching the polymer emission.

The field dependent quenching was absent for the optimized P3TI:$PC_{71}BM$ system. This indicates that for this system, the energetic difference E_{D^*}-E_{CT} of 0.1 eV is enough to sufficiently inhibit repopulation of the polymer singlet excited state. We therefore attribute the differences in IQE for the P3TI:$PC_{71}BM$ and PTI-1:$PC_{61}BM$ systems primarily to their energetic differences in E_{D^*}-E_{CT}.

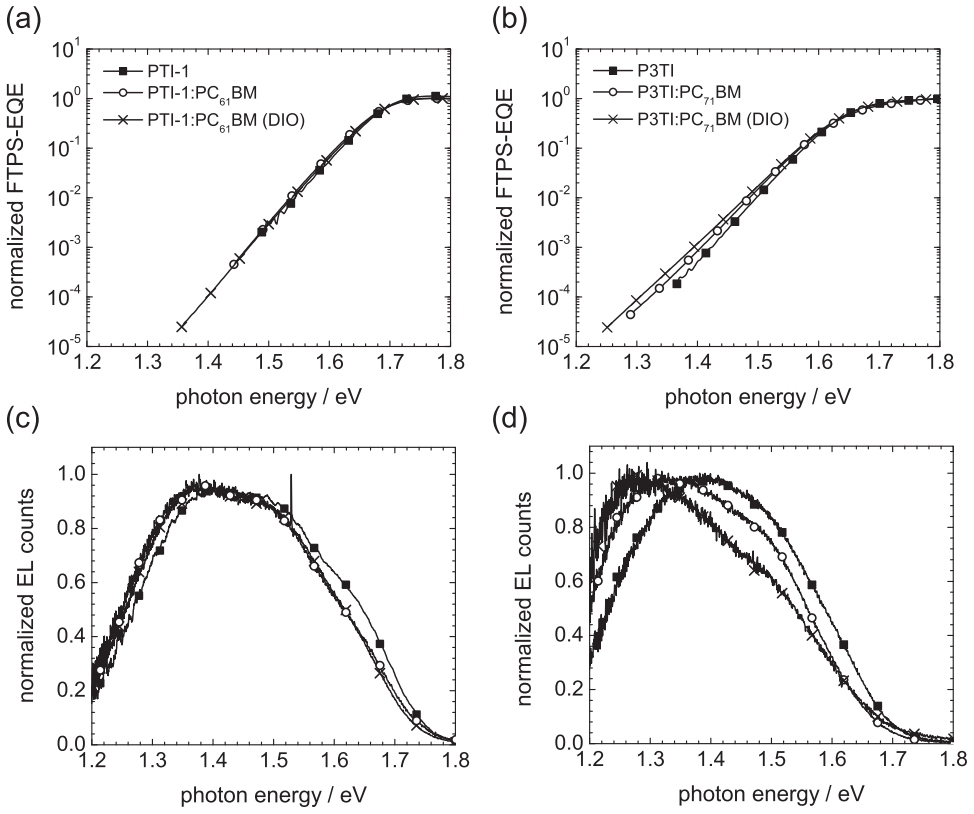

Figure 7. Normalized EQE and EL spectra in the low energy region for photovoltaic devices comprising pure polymers (squares) and blends prepared without DIO (circles) and with DIO (crosses). Highly sensitive EQE spectra are measured by FTPS and shown for (a) PTI-1 and (b) P3TI based devices. EL spectra are shown in panel (c) for PTI-1 and panel (d) for P3TI based devices.

Note that the method used to determine offset energies and "driving force" for electron transfer is superior to methods relying on estimations using frontier orbital energies (HOMO and LUMO), which do not take into account interfacial effects such as the CT state binding energy. Square wave voltammetry measurements are shown in supplementary Figure S3. They predict LUMO(D)-LUMO(A) offsets of about 0.2–0.3 eV for both the PTI-1:$PC_{61}BM$ and P3TI:$PC_{71}BM$ systems. For both systems, the offset value is considered to be in the range of the empirical lower limit for efficient electron transfer from polymer to fullerene.[8] Further, the use of highly sensitive EQE and EL spectra instead of relying on frontier orbital energies, permits a more detailed investigation of the losses present at V_{oc}, as presented in the next paragraph.

5.2. V_{oc} of Photovoltaic Devices Comprising Pure and Blend Films

We will here outline a detailed investigation on how the low energy (CT) absorption and emission studied in the previous paragraph relates to V_{oc}. Open circuit is reached when the flux of photo-generated free charge carriers is opposite but equal in magnitude to the flux of recombination of the free charge carriers.[47,48] This simple premise is valid for most types of photovoltaic cells (dye cells, inorganic solar cells) and is experimentally verified also for organic solar cells.[49]

A maximum V_{oc} will be achieved when the free carrier recombination is minimized. Since any absorbing species must also emit light, this radiative recombination cannot be avoided. Considering radiative recombination only, theoretical considerations,[16,50,51] result in the following formula for the maximum obtainable $V^{rad}{}_{oc}$ under solar illumination and radiative recombination only.

$$V_{oc}^{rad} = \frac{kT}{q} \ln\left(\frac{J_{sc}}{J_0^{rad}}\right) \tag{2}$$

With the expressions for J_{sc} and $J^{rad}{}_0$ given by

$$J_{sc} = q \int E\,QE(E)\varphi_{AM1.5}(E)dE \tag{3}$$

$$J_0^{rad} = q \int E\,QE(E)\varphi_{BB}^{T}(E)dE \tag{4}$$

Hereby is q the elementary charge, $\phi_{AM1.5}(E)$ is the standard AM1.5 solar illumination spectrum and $\phi^{T}{}_{BB}(E)$ the black body spectrum at the temperature T of the solar cell.

Because of the exponential decaying nature of $\phi^{T}{}_{BB}(E)$ for E >> kT, the main contributor to $J^{rad}{}_0$ is the low energy part of the EQE spectrum, hence our efforts using the highly sensitive FTPS, focusing on this part. Note that the $\frac{J_{sc}}{J_0^{rad}}$ ratio is only

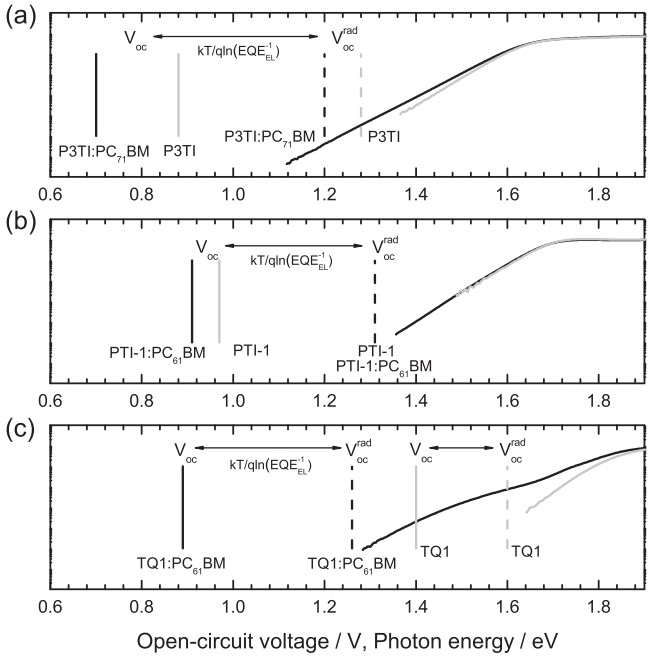

Figure 8. Schematic representation of calculated V_{oc}^{rad} and measured V_{oc} for photovoltaic devices consisting of pure polymer and blend active layers. The spectral shape of the low energy EQE(E) spectrum is indicated for every material. Panel (a) contains data for P3TI and P3TI:$PC_{71}BM$, panel (b) for PTI-1 and PTI-1:$PC_{61}BM$ and panel (c) for TQ1 and TQ1:$PC_{61}BM$ as an example of a high E_{D^*}-E_{CT} system with pronounced CT absorption band.

dependent on the spectral shape of EQE and not on its absolute value.

Non-radiative recombination pathways will lead to a lower V_{oc} as compared to V^{rad}_{oc}. This loss can be quantified as[10,11,13,50,51]

$$V_{oc} = V_{oc}^{rad} + \frac{kT}{q} \ln (EQE_{EL}) \quad (5)$$

The presence of non-radiative recombination will result in an EQE_{EL} smaller than 1, making the second term on the right hand side of equation (5) smaller or equal to 0. For polymer:fullerene solar cells the EL is dominated by CT emission with typically $EQE_{EL} < 10^{-6}$, resulting in a loss in V_{oc} due to non-radiative recombination >0.36 V at room temperature.[11]

Calculated V^{rad}_{oc} and measured V_{oc}, for pure PTI-1 and P3TI and optimized PTI-1:$PC_{61}BM$ and P3TI:$PC_{71}BM$ photovoltaic devices are depicted in **Figure 8**a and (b), together with the low energy EQE spectrum used to calculate J_{sc} and J^{rad}_0 from Equation (3) and Equation (4) and V^{rad}_{oc} using Equation (2). For the P3TI and P3TI:$PC_{71}BM$ blend, the measured V_{oc} is respectively 0.4 and 0.5 V lower than the a calculated V^{rad}_{oc} of 1.28 V and 1.21 V resulting in 0.88 V and 0.70 V. Equation (4) predicts EQE_{EL} values of 2×10^{-7} and 5×10^{-9}, close to the measured values of 1×10^{-7} and 5×10^{-9}, respectively, indicating the validity of this approach for quantifying losses at V_{oc}.[10,11]

For pure PTI-1 and PTI-1:PCBM devices, V^{rad}_{oc} is calculated to have the same value (1.31 V) since the low energy part of the EQE spectrum is similar for both devices. However, measured V_{oc} for the blend and pure material are different, respectively 0.92 and 0.96 V. We measured the EQE_{EL} for pure material and blend, which drops by an order of magnitude upon blending, from 2×10^{-6} to 2×10^{-7}. These values of EQE_{EL} correspond to the respective 0.35 and 0.4 V difference between V_{oc} and V^{rad}_{oc}.

As a reference example of a typical, higher E_{D^*}-E_{CT} system, data for a poly[2,3-bis-(3-octyloxyphenyl)quinoxaline-5,8-diyl-alt-thiophene-2,5-diyl] (TQ1):$PC_{61}BM$ device is included in Figure 8c. For devices based on TQ1, previously, a power conversion efficiency of up to 6% and a maximum EQE of ~60% were obtained.[52] As opposed to the isoindigo based polymers, a pronounced CT band is visible in the low energy part of the EQE spectrum of the TQ1:$PC_{61}BM$ blend, resulting in a quite large E_{D^*}-E_{CT} of ~0.4 eV. Consequently, for this material system, the difference between the calculated V^{rad}_{oc} for the pure polymer (1.6 V) and V^{rad}_{oc} for the blend, is quite large (1.26 V). This is also reflected in the actually obtained V_{oc}, which is 1.4 V for the pure material and 0.89 V for the blend. The difference between V^{rad}_{oc} and V_{oc} predict losses due to non-radiative recombination (Equation 4) of respectively 4×10^{-4} and 5×10^{-7} closely corresponding to measured EQE_{EL} values of 1×10^{-3} respectively 9×10^{-7}.

From the above we conclude that for the PTI-1:$PC_{61}BM$ system, V_{oc} is the most optimized of the material systems depicted in Figure 8. In this system, V_{oc} can *only* be increased by removing non-radiative recombination pathways. Future research efforts are needed to identify these radiationless decay pathways. They might e.g. involve sub-gap localized electronic states or triplet states on the polymer or fullerene. A major question remains if such low EQE_{EL} values as observed here and in previous work,[10,11] are intrinsic to polymer:fullerene blends which produce a high yield of free charge carriers.

For the high voltage P3TI:$PC_{61}BM$ system, unfortunately, the absence of a E_{D^*}-E_{CT} difference affects the IQE and lowers it to 45%. With a slightly higher E_{D^*}-E_{CT} of ~0.1 eV, an IQE of 87% for the optimized P3TI:$PC_{71}BM$ blend could be obtained. This however, is accompanied with unavoidable loss in V_{oc}, due to radiative CT state recombination.

7. Conclusions

Photocurrent and voltage losses in polymer:fullerene blends based on isoindigo containing polymers (P3TI and PTI-1) were studied in detail. We measure the energetic loss E_{D^*}-E_{CT} due to the electron transfer directly via FTPS and EL measurements, rather than using LUMO(D)-LUMO(A) offset energy levels obtained by electrochemistry. This approach can be used directly on blend films, and exciton binding energies and other interfacial effects are taken into account.

The polymer:fullerene blends studied in this work are of special relevance since we find losses E_{D^*}-E_{CT} which much lower than typically observed for polymer:fullerene systems: For P3TI:$PC_{71}BM$ blends we find a E_{D^*}-E_{CT} of 0.1 eV while for the PTI-1:$PC_{61}BM$ system we find an even lower E_{D^*}-E_{CT} (~0.0 eV), resulting in a V_{oc} of 0.7 and 0.92 eV respectively. Even though their E_{D^*}-E_{CT} differences are low, we find for P3TI:$PC_{71}BM$ an IQE of 87% and for the PTI-1:$PC_{61}BM$ system an IQE of 45%. Morphology and field dependent PL quenching indicates

that the lower IQE for the PTI-1 system is due to an interfacial effect related to the very low E_{D^*}-E_{CT}, facilitating repopulation of the donor exciton, and not due to a too coarse morphology. However, the fact that such a respectable IQE value can still be obtained with minimized losses in the electron transfer step, is surprising. We hope this encourages the search for systems with very low E_{D^*}-E_{CT} and even higher IQEs.

8. Experimental Section

Variable angle spectroscopic ellipsometry (VASE): VASE was performed on spin-coated thin films using a RC2 instrument from J.A. Woolam Co., Inc. Incident angles were varied in steps of ten degrees from 45° to 75°. Layers of PTI-1 and P3TI and their blends with $PC_{61}BM$ and $PC_{71}BM$ were spincoated on silicon substrates with a 100 nm or 1 nm thick oxide layer. The software Complete Ease from J.A. Woolam Co., Inc was used to model the VASE measurements. A Cauchy model in the transparent IR region was used to determine the thickness of the thin films. Tauc-Lorentz oscillators were used to model the optical constants.

Device fabrication and characterization: The BHJ solar cells were fabricated using a device architecture glass/ITO/PEDOT:PSS(40 nm)/active layer/LiF(0.6 nm)/Al(80 nm). The ITO covered glass substrates were cleaned by detergent and acetone prior to TL-1 (a mixture of water, ammonia (25%), and hydrogen peroxide (28%) (5:1:1 by volume)) treatment. PEDOT:PSS was spin-cast onto the cleaned substrate and heated for 10 minutes at 120 °C. Then, the substrates were transferred into a glove box filled with N_2. The active layers were spin-coated from *o*-DCB (with and without 2.5% DIO) solutions on top of the PEDOT:PSS coated ITO glass substrates. The substrates were moved into a vacuum chamber where 0.6 nm LiF and 80 nm Al were thermally evaporated at a pressure less than 4×10^{-6} mbar. Current density–voltage (*J–V*) curves, used to determine J_{sc}, V_{oc}, FF and PCE, were measured by using Keithley 2400 Source Meter under illumination of AM 1.5 filtered light, with intensity of 100 mW cm^{-2} (solar simulator Model SS-50A, Photo Emission Tech., Inc.). EQE spectra were obtained using a Newport Merlin lock-in with the solar cells illuminated with chopped monochromatic light through the ITO side. The thickness of the active layers was measured by a surface profiler (Dektak 6M). Reflectance of solar cells was measured with a UV/VIS spectrometer (Lambda 950) equipped with an integrating sphere. This reflectance and the optical constants, obtained using VASE were used in a transfer matrix model to determine the IQE.

AFM and TEM: The films for measuring AFM and TEM were spin-coated from *o*-DCB or *o*-DCB:2.5% (by volume) DIO solutions on top of PEDOT:PSS covered clean ITO glass substrates under the same conditions as for the deposition of the active layers in solar cells. AFM was performed directly on these films, with a Dimension 3100 system (Digital Instruments/Veeco) by using Antimony (n) doped Silicon cantilevers (SCM-PIT, Veeco) in tapping mode. For preparing TEM samples, PEDOT:PSS was used as the sacrificial layer, by dissolving it in water during the lift-off process. The films were put in vacuum over night, before measurement. Then, the active layers were placed onto a copper grid, used as sample support. TEM images were recorded with a Philips CM20/ST transmission electron microscope operated at 200 kV.

PL and EL measurement: EL, PL and field-dependent PL spectra were obtained with an Andor spectrometer (Shamrock sr-303i-B, coupled to a Newton EMCCD detector) and both pure polymers and blends based devices connected to an external current/voltage source for the measurements of EL and field-dependent PL spectra. A red CW He-Ne 632 nm laser with an intensity of 2 mW cm^{-2} was used as pumping light source for the absolute PL and field-dependent PL measurements.

EQE_{EL} measurements: The EQE_{EL} spectra were obtained from a home built system comprising a Hamamatsu silicon photodiode 1010B, a Keithley 2400 for supplying voltages and recording injected current, and a Keithley 485 for measuring the emitted light intensity.

FTPS-EQE measurement: FTPS-EQE was carried out using a Vertex 70 from Bruker optics, equipped with a QTH lamp, quartz beamsplitter and external detector option. A low noise current amplifier (SR570) is used to amplify the photocurrent produced upon illumination of the photovoltaic devices with light modulated by the FTIR. The output voltage of the current amplifier is fed back into the external detector port of the FTIR, in order to be able to use the FTIR's software to collect the photocurrent spectrum.

Supporting Information

Supporting Information is available from the Wiley Online Library or from the author.

Acknowledgements

The authors K.V. and Z. M. made equal contributions to the work. We gratefully acknowledge funding from the Swedish Energy Agency through the program Tandem, as well as the Swedish Research Council (VR), VINNOVA and the Knut and Alice Wallenberg foundation for providing equipment financing.

Received: March 2, 2012
Revised: April 7, 2012
Published online: May 7, 2012

[1] Y. Liang, Z. Xu, J. Xia, S.-T. Tsai, Y. Wu, G. Li, C. Ray, L. Yu, *Adv. Mater.* **2010**, *22*, E135.
[2] M. A. Green, K. Emery, Y. Hishikawa, W. Wata, *Prog. Photovolt: Res. Appl.* **2011**, *19*, 84.
[3] S. H. Park, A. Roy, S. Beaupré, S. Cho, N. Coates, J. S. Moon, D. Moses, M. Leclerc, K. Lee, A. J. Heeger, *Nature Phot.* **2009**, *3*, 297.
[4] H.-Y. Chen, J. Hou, S. Zhang, Y. Liang, G. Yang, Y. Yang, L. Yu, Y. Wu, G. Li, *Nature Phot.* **2009**, *3*, 649.
[5] C. Deibel, V. Dyakonov, *Rep. Prog. Phys.* **2010**, *73*, 096401.
[6] T. M. Clarke, J. R. Durrant, *Chem. Rev.* **2010**, *110*, 6736.
[7] M. C. Scharber, D. Mühlbacher, M. Koppe, P. Denk, C. Waldauf, A. J. Heeger, C. J. Brabec, *Adv. Mater.* **2006**, *18*, 789. G. Dennler, M. C. Scharber, T. Ameri, P. Denk, K. Forberich, C. Waldauf, C. J. Brabec, *Adv. Mater.* **2008**, *20*, 579.
[8] G. Dennler, M. C. Scharber, C. J. Brabec, *Adv. Mater.* **2009**, *21*, 1323.
[9] D. Veldman, S. C. J. Meskers, R. A. J. Janssen, *Adv. Funct. Mater.* **2009**, *19*, 1939.
[10] K. Vandewal, K. Tvingstedt, A. Gadisa, O. Inganas, J. V. Manca, *Nat. Mater.* **2009**, *8*, 904.
[11] K. Vandewal, K. Tvingstedt, A. Gadisa, O. Inganas, J. V. Manca, *phys. Rev. B* **2010**, *81*, 125204.
[12] K. Vandewal, A. Gadisa, W. D. Oosterbaan, S. Bertho, F. Banishoeib, I. Van Severen, L. Lutsen, T. J. Cleij, D. Vanderzande, J. V. Manca, *Adv. Funct. Mater.* **2008**, *18*, 2064.
[13] K. Vandewal, K. Tvingstedt, J. V. Manca, O. Inganas, *IEEE J. Sol. Top. Quant. Elec.* **2010**, *16*, 1676.
[14] D. Veldman, O. Ipek, S. C. J. Meskers, J. Sweelssen, M. M. Koetse, S. C. Veenstra, J. M. Kroon, S.S. van Bavel, J. Loos, R. A. J. Janssen, *J. Am. Chem. Soc.* **2008**, *130*, 7721.
[15] K. Tvingstedt, K. Vandewal, A. Gadisa, F. Zhang, J. Manca, O. Inganas, *J. Am. Chem. Soc.* **2009**, *131*, 11819.
[16] M. A. Faist, T. Kirchartz, W. Gong, R. S. Ashraf, I. McCulloch, J. C. de Mello, N. J. Ekins-Daukes, D. D. C. Bradley, J. Nelson, *J. Am. Chem. Soc.* **2012**, *134*, 685.

[17] F. He, L. Yu, *J. Phys. Chem. Lett.* **2011**, *2*, 3102.
[18] J. L. Bredas, J. E. Norton, J. Cornil, V. Coropceanu, *Acc. Chem. Res.* **2009**, *42*, 1691.
[19] H. OhkitaS. Cook, Y. Astuti, W. Duffy, S. Tierney, W. Zhang, M. Heeney, I. McCulloch, J. Nelson, D. D. C. Bradley, J. R. Durrant, *J. Am. Chem. Soc.* **2008**, *130*, 3030.
[20] S. Shoaee, T. M. Clarke, C. Huang, S. Barlow, S. R. Marder, M. Heeney, I. McCulloch, J. R. Durrant, *J. Am. Chem. Soc.* **2010**, *132*, 12919.
[21] J. Lee, K. Vandewal, S. R. Yost, M. E. Bahlke, L. Goris, M. A. Baldo, J. V. Manca, T. Van Voorhis, *J. Am. Chem. Soc.* **2010**, *132*, 11878.
[22] R. D. Pensack, J. B. Asbury, *J. Phys. Chem. Lett.* **2010**, *1*, 2255.
[23] R. D. Pensack, J. B. Asbury, *Chem. Phys. Lett.* **2010**, *515*, 197.
[24] S. Westenhoff, I. A. Howard, J. M. Hodgkiss, K. R. Kirov, H. A. Bronstein, C. K. Williams, N. C. Greenham, R. H. Friend, *J. Am. Chem. Soc.* **2008**, *130*, 13653.
[25] D. Di Nuzzo, A. Aguirre, M. Shahid, V. S. Gevaerts, S. C. J. Meskers, R. A. J. Janssen, *Adv. Mater.* **2010**, *22*, 4321.
[26] C. Dyer-Smith, L. X. Reynolds, A. Bruno, D. D. C. Bradley, S. A. Haque, J. Nelson, *Adv. Funct, Mater.* **2010**, *20*, 2701.
[27] E. Wang, Z. Ma, Z. Zhang, K. Vandewal, P. Henriksson, O. Inganas, F. Zhang, M. Andersson, *J. Am. Chem. Soc.* **2011**, *133*, 14244.
[28] Z. Ma, E. Wang, K. Vandewal, M.R. Andersson, F. Zhang, *Appl. Phys. Lett.* **2011**, *99*, 143302.
[29] P. M. Beaujuge, C. M. Amb, J. R. Reynolds, *Acc. Chem. Res.* **2010**, *43*, 1396.
[30] N.-K. Persson, M. Sun, P. Kjellberg, T. Pullerits, O. Inganas, *J. Chem. Phys.* **2005**, *123*, 204718.
[31] E. Wang, Z. Ma, Z. Zhang, P. Henriksson, O. Inganas, F. Zhang, M. R. Andersson, *Chem. Comm.* **2011**, *47*, 4908.
[32] G. Burkhard, E. T. Hoke, M. D. McGehee, *Adv. Mater.* **2010**, *22*, 3293.
[33] M. Tong, N. E. Coates, D. Moses, A. J. Heeger, S. Beaupre, M. Leclerc, *Phys. Rev. B* **2010**, *81*, 125210.
[34] J. Peet, J. Y. Kim, N. E. Coates, W. L. Ma, D. Moses, A. J. Heeger, G. C. Bazan, *Nature. Mater.* **2007**, *6*, 497.
[35] J. C. Bijleveld, V. S. Gevaerts, D. Di Nuzzo, M. Turbiez, S. G. J. Mathijssen, D. M. de Leeuw, M. M. Wienk, R. A. J. Janssen, *Adv. Mater.* **2010**, *22*, E242.
[36] M.-S. Su, C.-Y. Kuo, M.-C. Yuan, U.-S Jeng, C.-J. Su, K.-H. Wei, *Adv. Mater.* **2011**, *23*, 3315.
[37] M. Hallermann, I. Kriegel, E. Da Como, J. M. Berger, E. von Hauff, J. Feldmann, *Adv. Funct. Mater.* **2009**, *19*, 3662.
[38] M. C. Scharber, C. Lungenschmied, H.-J. Egelhaaf, G. Matt, M. Bednorz, T. Fromherz, J. Gao, D. Jarzab, M. A. Loi, *Energy Environ. Sci.* **2011**, *4*, 5077.
[39] J. Kern, S. Schwab, C. Deibel, V. Dyakonov, *Phys. Status Solidi-R* **2011**, *5*, 364.
[40] K. Tvingstedt, K. Vandewal, F. Zhang, O. Inganas, *J. Phys. Chem. C* **2010**, *144*, 21824.
[41] C. Deibel, T. Strobel, V. Dyakonov, *Adv. Mater.* **2010**, *22*, 4097.
[42] S. Chambon, R. Mens, K. Vandewal, E. Clodic, M. Scharber, L. Lutsen, J. Gelan, J. Manca, D. Vanderzande, P. Adriaensens, *Sol. Energy Mater. Sol. Cells* **2012**, *96*, 210.
[43] E. Wang, J. Bergqvist, K. Vandewal, Z. Ma, L. Hou, S. Hellström, C. Müller, O. Inganäs, F. Zhang, M. R. Andersson, **2012**, Unpublished.
[44] F. Piersimoni, S. Chambon, K. Vandewal, R. Mens, T. Boonen, A. Gadisa, M. Izquierdo, S. Filippone, B. Ruttens, J. D'Haen, N. Martin, L. Lutsen, D. Vanderzande, P. Adriaensens, J. V. Manca, *J. Phys. Chem. C* **2011**, *115*, 10873.
[45] J. J. Benson-Smith, L. Goris, K. Vandewal, K. Haenen, J. V. Manca, D. Vanderzande, D. D. C. Bradley, J. Nelson, *Adv. Funct. Mater.* **2007**, *17*, 451.
[46] M. A. Loi, S. Toffanin, M. Muccini, M. Forster, U. Scherf, M. Scharber, *Adv. Funct. Mater.* **2007**, *17*, 2111.
[47] P. Wurfel, in *Physics of solar cells: from basic principles to advanced concepts*, 1st edition, Wiley-VCH, Weinheim, Germany **2009**.
[48] J. Nelson, *The physics of solar cells*, 1st edition, Imperial College Press, London **2003**.
[49] A. Maurano, R. Hamilton, C. G. Shuttle, A. M. Ballantyne, J. Nelson, B. O'Regan, W. Zhang, I. McCulloch, H. Azimi, M. Morana, C. J. Brabec, J. R. Durrant, *Adv. Mater.* **2010**, *22*, 4987.
[50] U. Rau, *Phys. Rev. B* **2007**, *76*, 085303.
[51] T. Kirchartz, U. Rau, *J. Appl. Phys.* **2007**, *102*, 104510.
[52] E. Wang, L. Hou, Z. Wang, S. Hellström, F. Zhang, O. Inganäs, M. R. Andersson, *Adv. Mat.* **2010**, *22*, 5240.